



OPEN ACCESS

EDITED BY
Daoyang Yuan,
Lanzhou University, China

REVIEWED BY
Bouhadad Youcef,
National Earthquake Engineering
Center (CGS), Algeria
Yujiang Li,
Ministry of Emergency Management,
China

*CORRESPONDENCE
Guihua Chen,
guihuachen@ies.ac.cn

SPECIALTY SECTION
This article was submitted to Structural
Geology and Tectonics,
a section of the journal
Frontiers in Earth Science

RECEIVED 15 June 2022
ACCEPTED 08 August 2022
PUBLISHED 06 September 2022

CITATION
Chen G, Li Z and Huang X (2022), Late
Quaternary faulting and
paleoearthquakes along the northern
section of the Bayanhaote fault and their
implications for
regional seismotectonics.
Front. Earth Sci. 10:970192.
doi: 10.3389/feart.2022.970192

COPYRIGHT
© 2022 Chen, Li and Huang. This is an
open-access article distributed under
the terms of the [Creative Commons
Attribution License \(CC BY\)](https://creativecommons.org/licenses/by/4.0/). The use,
distribution or reproduction in other
forums is permitted, provided the
original author(s) and the copyright
owner(s) are credited and that the
original publication in this journal is
cited, in accordance with accepted
academic practice. No use, distribution
or reproduction is permitted which does
not comply with these terms.

Late Quaternary faulting and paleoearthquakes along the northern section of the Bayanhaote fault and their implications for regional seismotectonics

Guihua Chen*, Zhongwu Li and Xiongnan Huang

State Key Laboratory of Earthquake Dynamics, Institute of Geology, China Earthquake Administration, Beijing, China

Analysis of the late Quaternary activity and paleoseismicity of the Bayanhaote fault is critical because it is part of the frontier of the propagating Tibetan Plateau and the boundary between the Alxa and Ordos blocks, and the development of a regional seismotectonic model surrounding the Helan Mountains is crucial. We studied offset landforms and paleoearthquakes along the northern section of the Bayanhaote fault and found that it deformed dextrally, with a slight reverse slip to the east. A channel and a deluvial edge on the alluvial terrace, aged between 56.28 ± 4.04 ka and 82.2 ± 5.78 ka, are right-laterally offset and a sag pond formed on the east side of the fault scarp. We calculated a dextral slip rate of 1.0–2.4 mm/a. Three surface-rupturing paleoearthquakes were discovered in the reversely offset strata in a trench south of Sumutu village. We infer that these three earthquakes might be a portion of surface-rupturing earthquakes by comparing them with documented paleoearthquake data along the southern half of the Bayanhaote fault. We established a regional seismotectonic model around the Helan Mountains using our new and published geological and geophysical data. The seismic risk along the dextral Bayanhaote fault to the west of the Helan Mountains is also substantial. The dextral Bayanhaote fault west of the Helan Mountains and the normal fault system in the east constitute the active boundary belt between the Alxa and Ordos blocks.

KEYWORDS

Bayanhaote fault, active fault, late Quaternary, regional seismotectonics, Ordos block, Alxa block

Introduction

The vast Tibetan Plateau was formed by the collision of India and Eurasia, and it is still expanding northward under this tectonic regime, which profoundly shaped the intracontinental tectonic framework and controlled seismicity in western China

(Tapponnier et al., 2001; Yuan et al., 2013). The Alxa block is a tectonic and seismically active area where the Tibetan Plateau interacts with the Ordos and Xingmeng blocks during the outward expansion of the northeastern margin of the Tibetan Plateau (Research Group on Active Fault System around Ordos Massif, 1988; Deng et al., 1999; Huang et al., 2012; Yang and Dong,

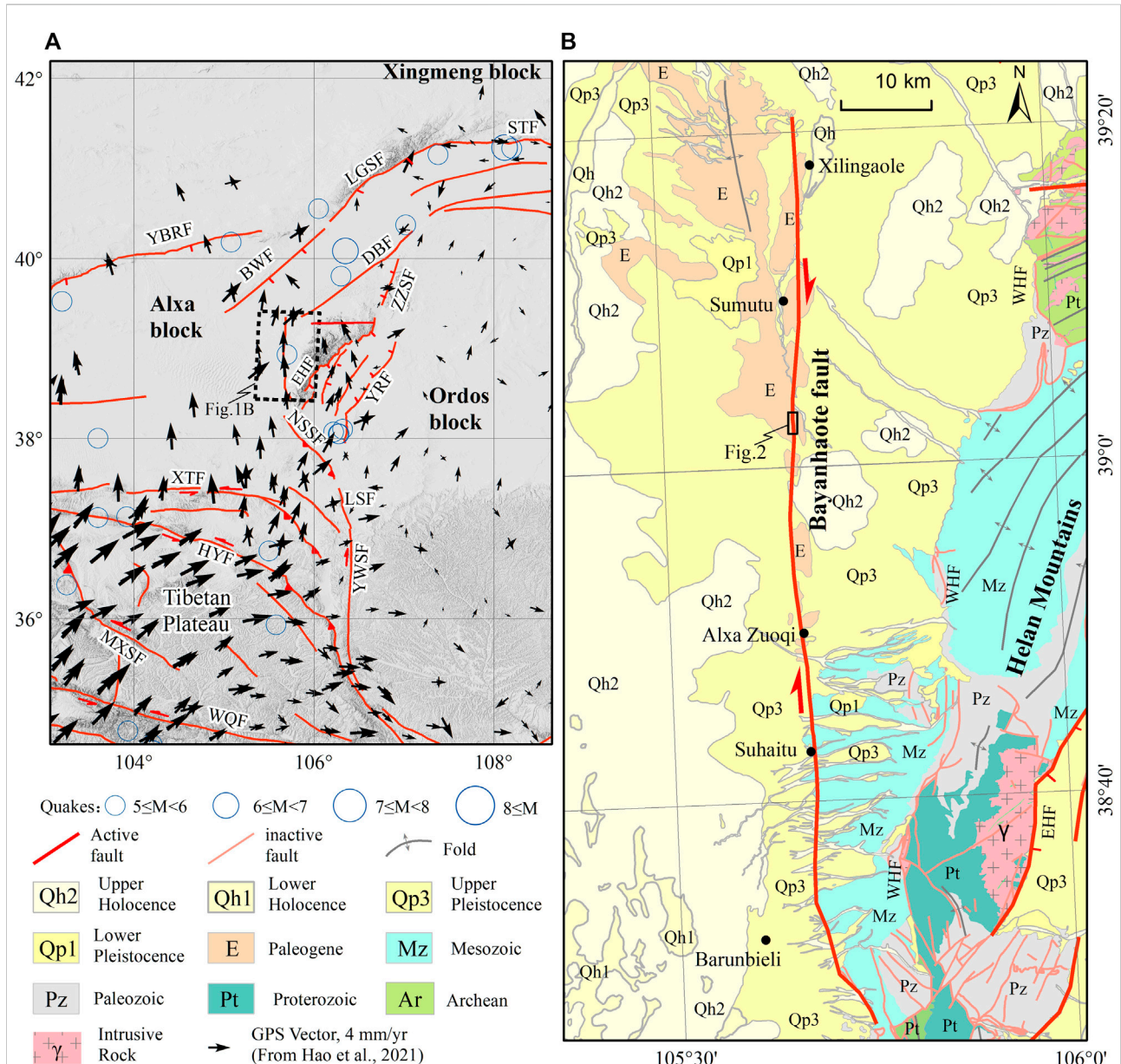


FIGURE 1 Regional geological setting of the Bayanhaote fault. (A) Major active faults, earthquakes, and GPS velocity fields in the western margin of Ordos (fault modified from Xu et al., 2016; earthquake catalog from China Earthquake Network Center; GPS velocity with respect to the Ordos block from Hao et al. (2021)). (B) Structure of the Bayanhaote fault with geological background (geological data from 1: 250,000 scale public geological map via geocloud. <http://geocloud.cgs.gov.cn>). BWF: Bayan Wula fault; EHF: East Helanshan fault; HYF: Haiyuan fault; LGSF: Langshan fault; LSF: Luoshan fault; MXSF: Maxianshan fault; NSSF: Niushoushan fault; STF: Seerteng fault; WHF: West Helanshan fault; WQF: West Qinlin fault; XTF: Xiangshan-Tianjingshan fault; YBRF: Yabrai fault; YWSF: Yunwushan fault; ZZSF: Zhuozishan fault.

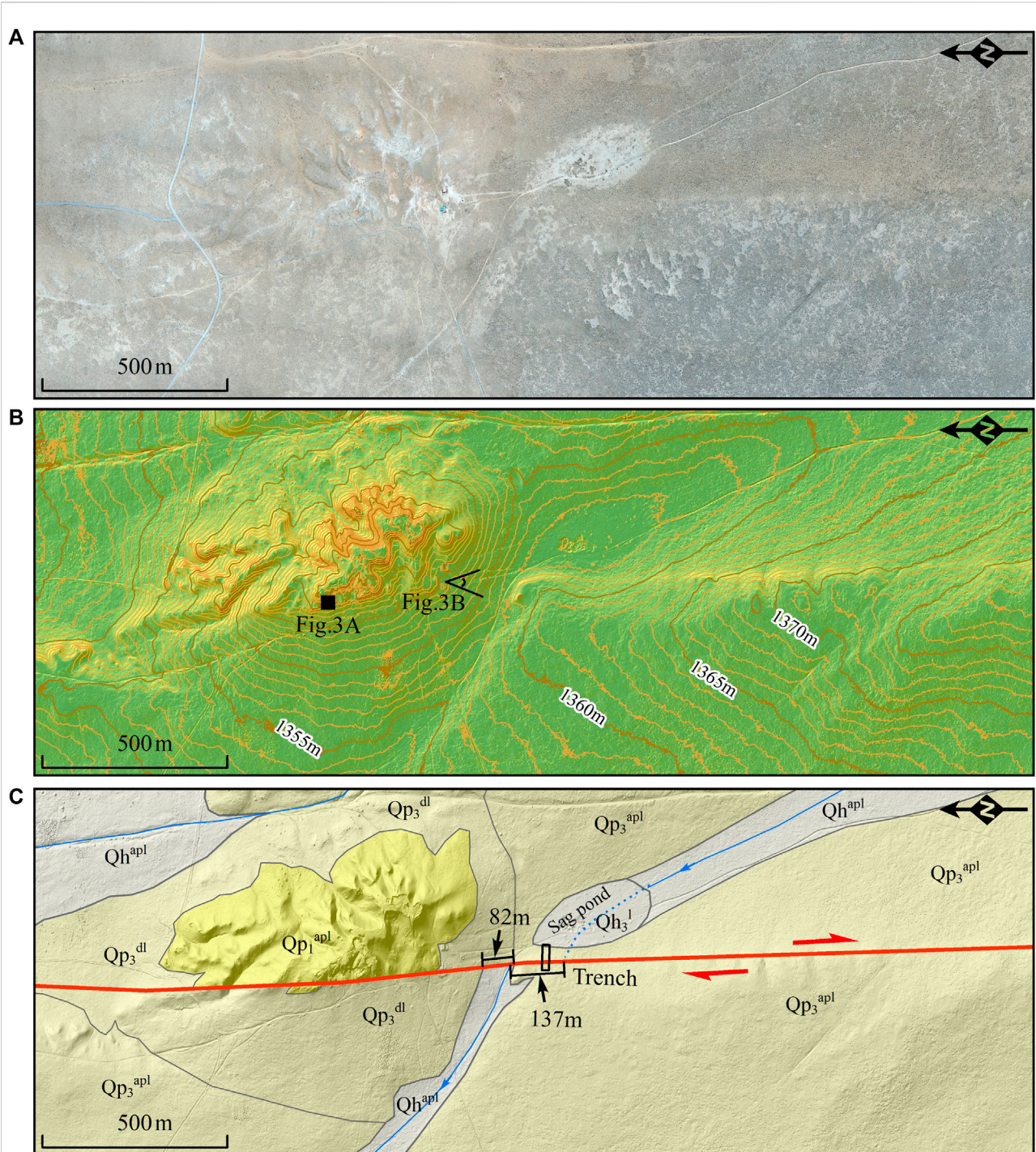
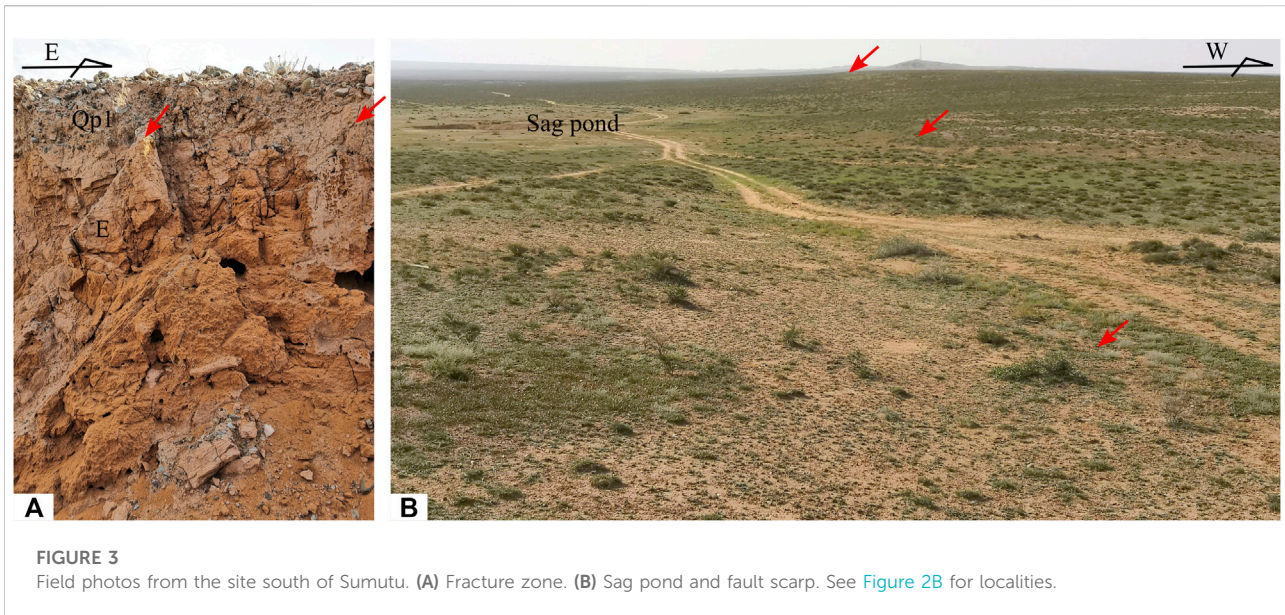


FIGURE 2
 Site south of Sumutu. (A) DOM in 5 cm resolution. (B) Shaded relief from DEM in 10 cm resolution. with contours. (C) Offset Geological map and offset landforms. Qh₃^{apl}: active sag pond sediment; Qh^{apl}: Holocene alluvial; Qp₃^{apl}: Late Pleistocene alluvial; Qp₃^{dl}: Late Pleistocene deluvial; Qp₁^{apl}: Early Pleistocene alluvial; Rectangle denotes the trench site.

2018; Zhang et al., 2021). The analysis of faulting and seismicity around Alxa is critical for understanding the deformation behavior and dynamics of intracontinental structures.

Since the Mesozoic Era, the eastern Alxa block has interacted with the Ordos block, resulting in the formation of several graben basins, such as the Bayanhaote, Jilantai, and Yinchuan basins and



the Helan Mountains, which are bordered by these basins (Liu et al., 2010; Yang and Dong, 2018; Ma and He, 2019). A series of active faults developed between the basins and mountains and generated a series of strong historical earthquakes (Figure 1A). Certain faults have been investigated around the Yinchuan Graben, such as the East Helanshan, Yinchuan–Pingluo, and Yellow River faults (Middleton, et al., 2016a; Middleton, et al., 2016b; Lei, 2016; Wei et al., 2021); yet several faults remain unstudied (Zhang et al., 2021). Clarifying the late Quaternary activity of these faults and the occurrence of paleoearthquakes is critical for establishing a regional seismotectonic model. It provides the foundational data for analyzing intracontinental structures in this region, identifying seismogenic sources, and mitigating disasters caused by strong earthquakes.

The Bayanhaote fault is a major active fault in this region that has received little attention, possibly because the fault activated within the Bayanhaote Basin after its formation (Liu and Liu, 2002); however, the fault may be relatively weak in activity (Deng et al., 1999; Lei et al., 2022). In recent years, some scholars have conducted research and mapping work, particularly on the Bayanhaote fault, and they have published new data. However, evidence of late Quaternary activity of the fault is mainly concentrated in the southern section to the south of Alxa Zuoqi (Bayanhaote Town) (Jing et al., 2019; Bi et al., 2020; Lei et al., 2022). There is only evidence of synchronous gully twisting in the northern section, and reliable late Quaternary activity and paleoseismic data remain lacking. The current geology shows that the bedrock along the section to the north of Bayanhaote Town is Paleogene sandstone, whereas the exposed bedrock along the south section is Mesozoic strata (Figure 1B). This variation

may have resulted from the differential activity between the southern and northern sections of the Bayanhaote fault.

We carried out UAV aerial photogrammetry along the northern section of the Bayanhaote fault and obtained a high-precision and high-resolution digital elevation model (DEM) and orthophoto image (DOM) along the fault. The offset late Quaternary landform was analyzed at a site south of Sumutu village, and a trench was excavated, revealing the latest activity and paleoearthquake history of the northern section of the Bayanhaote fault.

Regional tectonics and seismicity

In some studies, the Bayanhaote fault within the Bayanhaote Basin is sometimes referred to as the West Helanshan fault, also known as the fault along the eastern boundary of the basin. In the research of the pre-Cenozoic structure, the Bayanhaote fault is considered a hidden fault in the basin, whereas the West Helanshan fault is a high-angle normal boundary fault between the Bayanhaote Basin and the Helan Mountains (Liu and Liu, 2002; Yang and Dong, 2018; Zhang et al., 2021). Some scholars refer to the active fault crossing Bayanhaote Town (Alxa Zuoqi), the target fault of this study, as the Bayanhaote fault (Huang et al., 2012; Jing et al., 2019; Zhang et al., 2021), while others refer to it as the West Helanshan fault (Bi et al., 2020; Lei et al., 2022). The West Helanshan fault between the Helan Mountains and the Bayanhaote Basin is currently considered dormant owing to lack of data on its activity (Huang et al., 2012). To distinguish the fault within the basin from that along the piedmont, the Bayanhaote fault discussed in this study refers to

TABLE 1 Dating results from Optically Stimulated Luminescence (OSL) samples.

Sample ID	Depth (m)	U (ppm)	Th (ppm)	K (%)	Dose rate (Gy/ka)	Equivalent dose (Gy)	OSL AgeF (ka)
SMT-OSL-9	3.0	0.996 ± 0.02	3.76 ± 0.02	1.72 ± 0.01	2.27 ± 0.10	186.43 ± 10.55	82.2 ± 5.78
SMT-OSL-10	2.0	2.63 ± 0.04	9.77 ± 0.03	2.04 ± 0.01	3.36 ± 0.14	215.73 ± 11.14	64.19 ± 4.22
SMT-OSL-11	2.0	1.69 ± 0.03	5.75 ± 0.03	1.90 ± 0.01	2.75 ± 0.11	242.09 ± 13.56	87.94 ± 6.11
SMT-OSL-12	1.5	2.21 ± 0.02	7.78 ± 0.10	1.97 ± 0.01	3.09 ± 0.13	173.65 ± 10.28	56.28 ± 4.04
SMT-OSL-13	3.0	2.06 ± 0.02	8.62 ± 0.03	1.98 ± 0.01	3.07 ± 0.13	170.05 ± 6.22	55.33 ± 3.04
SMT-OSL-14	2.7	2.66 ± 0.02	8.24 ± 0.10	1.90 ± 0.01	3.11 ± 0.13	153.0 ± 4.63	49.16 ± 2.5
SMT-OSL-15	2.0	5.07 ± 0.02	12.1 ± 0.02	2.18 ± 0.03	4.19 ± 0.17	137.38 ± 7.45	32.79 ± 2.22
SMT-OSL-16	1.6	2.52 ± 0.03	6.54 ± 0.09	1.91 ± 0.02	3.01 ± 0.12	115.96 ± 5.45	38.51 ± 2.4
SMT-OSL-17	1.2	1.89 ± 0.02	8.02 ± 0.10	1.97 ± 0.01	3.04 ± 0.12	41.85 ± 2.87	13.76 ± 1.1
SMT-OSL-18	0.7	1.70 ± 0.02	8.22 ± 0.04	1.96 ± 0.02	3.02 ± 0.12	23.76 ± 0.8	7.86 ± 0.43

Samples were analyzed using the coarse-grained (90–150 μm) quartz single aliquot regenerative-dose (SAR) method (Murray and Wintle, 2000). The OSL dating method followed the process described by Chen et al. (2022). We applied a Central Age Model (CAM) to the samples.



the active fault that developed in the Bayanhaote Basin, which passes through Alxa Zuoqi, as shown in Figure 1B.

The Bayanhaote Basin and other basins around the western margin of Ordos experienced at least four tectonic events after their formation, and substantial tectonic activity was recorded

during the Yanshan and Himalayan movements. The latest major tectonic event occurred during the Miocene, with the formation of a series of NW-trending open folds and NE-trending strike-slip faults, which were related to the rapid uplift and expansion of the Tibetan Plateau (Liu et al., 2010; Yang and Dong, 2018; Ma

and He, 2019). According to the focal mechanism from seismic observations, the maximum compressional principal axis of the present stress field in the northern part of the western margin of Ordos is NE-trending (Sheng et al., 2015; Wang et al., 2015; Guo et al., 2017). According to the GPS velocity field, the Tibetan Plateau is obliquely compressed in the NE direction in the northern part of the western margin of Ordos, whereas the Alxa block moves northward relative to Ordos (Figure 1A).

The Bayanhaote fault extends from Xilingaole in the north to Barunbieli in a north–south strike; the strike then becomes eastward, with a total length of >100 km (Figure 1B). It was divided into three sections (Jing et al., 2019; Lei et al., 2022). South of Alxa Zuoqi, the Bayanhaote fault is exposed on alluvial fans to the west of the Helan Mountains. The Bayanhaote fault is associated with the folds north of Alxa Zuoqi. Cenozoic rocks are folded and intermittently distributed along the fault. The western plate of the fault is relatively uplifted, and a secondary sedimentary basin was formed on the east side of the West Helanshan fault (Figure 1B).

A study on the Quaternary activity of the Bayanhaote fault shows that the fault is mainly dextral strike–slip displaced Paleogene rocks for >800 m and gullies for 12–14 m in the northern section (Lei et al., 2022). The Holocene strike–slip rate in the southern section was 1.08 ± 0.1 mm/a, and the average slip rate was 1.38 ± 0.2 mm/a since the late Pleistocene Era (Jing et al., 2019). The vertical slip rate since the late Pleistocene Era was 0.64 mm/a, determined from an offset alluvial fan. Lei et al. (2022) reported a dextral slip rate of 0.2–0.4 mm/a for the southern section.

There were few instrumental records of strong earthquakes and no surface-rupturing historical earthquakes along the Bayanhaote fault. The maximum historical events occurred on 16 June 1991, near the city of Alxa Zuoqi. Well-constrained results on paleoearthquakes are still expected owing to the limited dating data. Lei et al. (2022) excavated three trenches in Xiaosuhaitu and reported three paleoearthquake events between 5.9 ± 0.4 ka and 6.2 ± 0.7 ka, between 13.0 ± 0.2 ka and 24.0 ± 2.0 ka, and >30.54–30.6 ka. Jing et al. (2019) reported that three paleoearthquake events occurred according to their trenches at ~ 3, 6.0, and 8–11 ka, with a recurrence interval of 3,000–4,000 years. Characteristic displacements of strong earthquakes were proposed from the statistics of displacements based on the DEM, which are a right-lateral slip of ~3 m and vertical displacement of ~1 m (Bi et al., 2020).

Offset landforms at the site south of Sumutu

Erosional landforms developed along the northern section of the Bayanhaote fault, which were accompanied by the uplift of Cenozoic strata. Linear fault scarps were observed along the fault traces. There are no widely distributed deposits or young

landforms that record the activities of the fault. Only a few Holocene rivers and their landforms passed through the fault, which might explain the lack of published data in this section. We discovered a sag pond south of Sumutu that recorded the latest deformation of the fault.

Weathered Paleogene red sandstone and its overlying early Pleistocene gravel layer were uplifted near the fault south of Sumutu (Figure 2), and secondary fractures and fault-damaged zones were developed (Figure 3A). The right-lateral offsetting fault prevents a gully from flowing through the fault from southeast to the west (Figure 2 and Figure 3B). The western plate of the fault is relatively uplifted, forming a linear fault scarp with a height of 3–4 m, and the beheaded gully was abandoned. The blocked gully on the eastern plate of the fault formed a sag pond that continuously stored deposits. At present, the northern boundary of the sag pond is almost aligned with the outlet, and the linear western boundary is approximately 274 m long along the fault scarp. Considering the sediment filling of the sag pond above the gully on the east side of the fault, we estimated the original gully centerline as the center point of the western boundary of the sag pond. Using the gully as a mark, we obtained a right-lateral offset of 137 m on the abandoned terrace at this site. The deluvial, eroded from the uplifted Paleogene sandstone and early Pleistocene gravel layers, covered on the late Pleistocene terraces. Taking the inflection line between the diluvial slope and the terrace as a mark, the offset is 82 m (Figure 2C).

In view of the terrace deposits on the western plate of the fault shown by the trench, the sediments were primarily alluvial deposits. The deposit on the top of the terrace belonged to the same horizon as the reddish-brown silty clay covered in the gravel layer exposed by the trench. The optically stimulated luminescence (OSL) sample SMT-OSL-12 collected in this silty layer was dated at 56.28 ± 4.04 ka (Table 1). The OSL sample SMT-OSL-9 from the alluvial sand layer 3.2 m below the surface was dated at 82.2 ± 5.78 ka. Therefore, we estimated the right-lateral slip rate to be 1.0–2.4 mm/a using the dextral offset of 137 m and 82 m, and the terrace age of between 56.28 ± 4.04 ka and 82.2 ± 5.78 ka.

Paleoearthquake trenching at the site south of Sumutu

We excavated a trench 23 m long and 3–4 m deep across the fault scarp on the west side of the sag pond at the site south of Sumutu. The north wall of the trench (Figure 4) showed that the deformation zone was approximately 18 m. West of fault F1, the uplift plate maintained its original sedimentary strata. The descending plate east of fault F3 continuously accumulated deposits with weak deformation. A series of secondary faults produce an asymmetric semi-flower structure in the deformation zone between faults F1 and F3. The deformation zone can be

divided into two domains based on deformation intensity and properties: the strike-slip zone between faults F1 and F2 is characterized by co-seismic strike-slip fractures and corresponding filling deposits, and the reverse zone between faults F2 and F3 is characterized by west-dipping reverse faults and colluvium in front of the scarp.

The strike-slip zone between faults F1 and F2 is approximately 9 m wide. The filling wedge adjacent to fault F1 is 5 m wide and filled with silt, which could be the result of a wide surface rupture caused by a strong earthquake. There are many vertical faults on both sides. At least two events were distinguished from the cutting relationship between the faults and strata. The filling wedge along fault F2 broke many times, which shows that the deformation in this strike-slip zone is very complex. In this strike-slip domain, the terrace began to suffer erosion after terrace sedimentation and abandonment. Without new deposits, the deformation history of the strike-slip could not be effectively recorded or revealed from the trench profile.

In the reverse zone between faults F2 and F3, the main deformation is concentrated in thrust fault F3, and the strata between faults F2 and F3 thrust eastward and tilt. The footwall of fault F3 receives accumulation from the hanging wall *via* short-distance transportation. The accumulated strata recorded the active history of fault F3.

The stratum units in the reverse zone include the following: yellow-brown silt (U1); yellow-brown silt with gravel (U2), in which the OSL sample SMT-OSL-18 is dated to 7.86 ± 0.43 ka; dark brown silt with gravels (U3), colluvial wedge accumulation; yellowish brown silt (U4), in which the OSL sample SMT-OSL-17 was dated to 13.76 ± 1.1 ka; dark brown sandy clay with gravels (U5), deposit in a filling wedge; yellow-brown silty clay (U6), in which the OSL sample SMT-OSL-15 was dated to 32.79 ± 2.22 ka; yellow-brown fine-silty sands with clay (U7), in which the OSL sample SMT-OSL-14 was dated to 49.16 ± 2.5 ka, and there was no abrupt variation between this layer and U6, which may be deposited under low hydrodynamic conditions in a long period of time and controlled by the filling process of sag pond and the climate change; dark brown gravel-bearing sandy clay (U8), deposit in a filling wedge; dark brown sandy clay with gravels (U9), deposit in a filling wedge; gray-brown coarse sands with gravels (U10); reddish-brown fine silt with gravels (U11), in which the OSL sample SMT-OSL-13 was dated to 55.33 ± 3.04 ka; reddish-brown silty clay (U12), in which the OSL sample SMT-OSL-12 was dated to 56.28 ± 4.04 ka; reddish brown gravel with silt (U13); dark brown sandy clay with gravels (U14), deposit in a filling wedge; yellowish-brown coarse sands with gravels (U15), in which the OSL sample SMT-OSL-11 was dated to 87.94 ± 6.11 ka; yellow-brown gravel with coarse sands (U16); yellow-brown gravel (U17); yellow-brown gravel with coarse sands (U18).

According to the change in sediment grain size, the strata revealed in the eastern part of the trench were divided into three sedimentary series from coarse to fine: U15–U12 is the lowest

sedimentary series from gravel to clay; U11–U7–U6 is a sedimentary series in the middle from silt with gravel to clay; and U4 and its upper layers comprise the uppermost sedimentary series, which is dominated by silt. U3 was a sandwiched layer of silt and gravel. Compared with the stable accumulation on the west side of fault F1, the sedimentary series east of fault F2 was transported under short-distance water flow from the terrace to the west. These sedimentary series were not correlated with regional climate change but were mainly controlled by local slope changes. The slope change corresponds to the fault scarp formed by local co-seismic dip slip. Therefore, the variations among the three sedimentary series may correspond to strong earthquakes, that is, the stratigraphic interfaces U12/U11 and U6/U4 represent two earthquakes with corresponding times between 56.28 ± 4.04 ka and 55.33 ± 3.04 ka and between 32.79 ± 2.22 ka and 13.76 ± 1.1 ka, respectively.

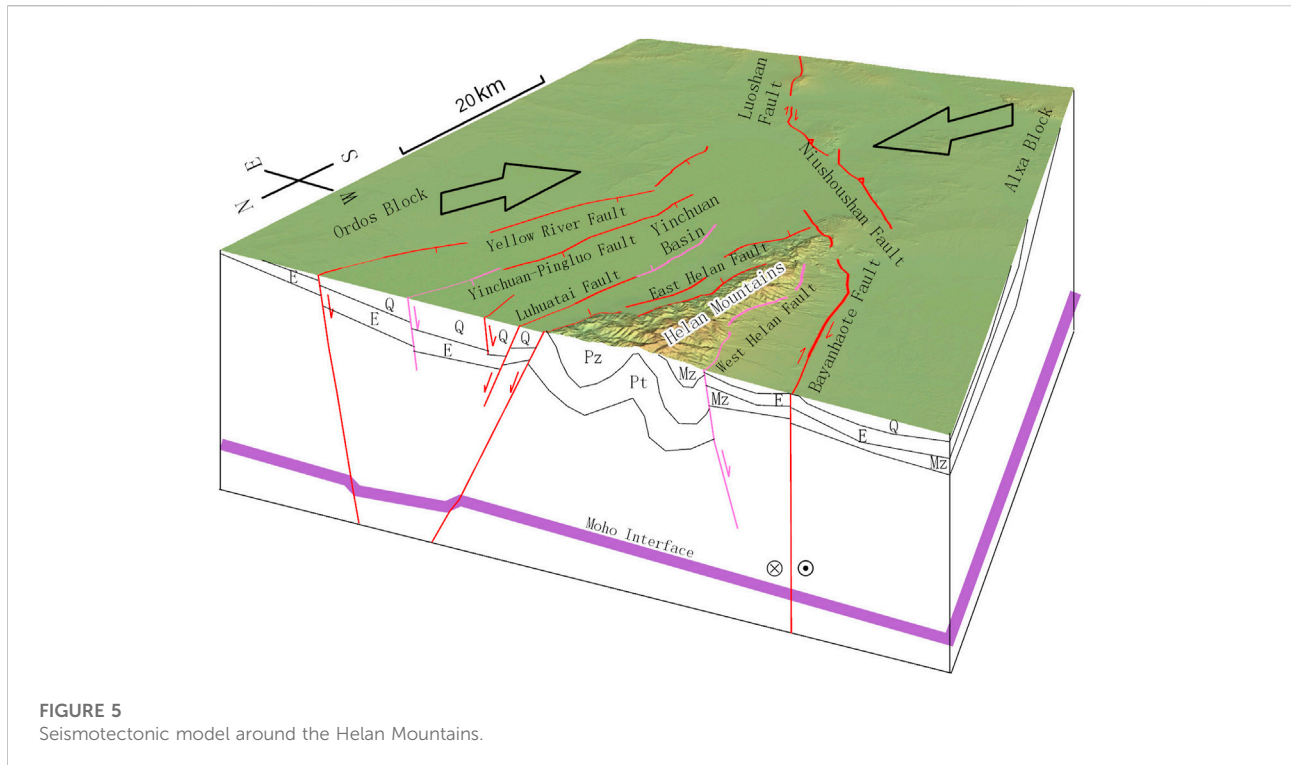
According to the layer thickness and occurrence, U11, U7, and U4 were thicker in the eastern plate of fault F3 than in the western plate. U3 is a colluvium wedge that is deposited rapidly in front of a fault scarp. After a ~ 0.29 -m offset of the top bedding of U4, a rapid deposit was formed on the foot of the fault scarp, which pinched out on the footwall (eastern plate) away from the fault. The dip-slip displacement of U12/U11 and U6/U4 along fault F3 is 1.08 and 0.64 m, respectively, which is consistent with the abovementioned sedimentary series analysis. The three different displacements of the three layers show that these layers recorded different times of co-seismic deformation.

With the constraint of OSL data for layers of event horizons, the three surface-rupturing strong earthquakes occurred between 56.28 ± 4.04 ka and 55.33 ± 3.04 ka, between 32.79 ± 2.22 ka and 13.76 ± 1.1 ka, and between 13.76 ± 1.1 ka and 7.86 ± 0.43 ka. According to the cumulative dip-slip, we calculated the dip slips of these three events to be 0.44, 0.35, and 0.29 m.

Discussion

Activity of the Bayanhaote fault and recurrence of strong earthquakes

According to the offset landforms at the site south of Sumutu and the deformation characteristics revealed from the trench, the northern section of the Bayanhaote fault was active in a right-lateral strike-slip with a certain reverse slip. The western plate of the fault is relatively uplifted, forming a fault scarp. The fault zone shows an asymmetric positive flower structure, as revealed by the trench at the site south of Sumutu. The main deformation zone is composed of vertical faults with a strong strike-slip. It also formed a thrust branch and fault scarp on the east side. The fault zone exposed from trenches at Suhaitu south of Alxa Zuoqi exhibits a negative flower structure (Lei, 2016; Jing et al., 2019; Lei et al., 2022). The southern section of the Bayanhaote fault deformed in dextral slip with normal slip. The fault scarp



shows relative uplift of the eastern plate along the southern section of the Bayanhaote fault. Although the entire Bayanhaote fault is dominated by strike-slip movement, it behaves differently in normal-slip in the southern section from reverse-slip in the north section.

In this study, we estimated the dextral strike-slip rate to be 1.0–2.4 mm/a in the northern section, which is much larger than that in the southern section, as reported by [Lei et al. \(2022\)](#). [Lei et al. \(2022\)](#) estimated the right-lateral strike-slip rate to be 0.2–0.4 mm/a in the southern section of the fault using the displaced terrace risers and the abandonment age of terraces. [Jing et al. \(2019\)](#) estimated the strike-slip rate to be 1.38 ± 0.2 mm/a using a 16.7-m offset of the lowest terrace with an abandonment age of ~12 ka, which is quite similar to the lower value of our result. We believe that this discrepancy may partially result from time constraints on the offset marks of landforms, especially for terrace risers ([Cowgill, 2007](#)). [Lei et al. \(2022\)](#) and [Jing et al. \(2019\)](#) used the abandonment ages of upper terraces. Considering the differences in fault properties, slip rates, and distribution of Neogene rocks between the southern and northern sections, we propose that the Bayanhaote fault deformed in a way similar to “the tearing” of the Alxa block with respect to the Helan Mountains, which implies the western plate of the northern section acts as the front of the active plate with compressing and uplifting, while the western plate of the

southern section acts as the tail of the active plate with stretching and subsidence.

As revealed by the dating data and structures from the trench at the site south of Sumutu, the Bayanhaote fault has been strongly deformed for 60,000 years in the northern section, and at least three strong surface-rupturing earthquakes have occurred. The most recent surface-rupturing earthquake occurred no earlier than the Holocene. We compared our paleoearthquake results in the northern section with those in the southern section reported by [Jing et al. \(2019\)](#) and [Lei et al. \(2022\)](#). The event between 13.76 ± 1.1 ka and 7.86 ± 0.43 ka is close to the events of 10.15–11.24 ka from [Lei \(2016\)](#) and 8.8–11.66 ka from [Jing et al. \(2019\)](#). The event between 32.79 ± 2.22 ka and 13.76 ± 1.1 ka is consistent with the event between 13.0 ± 0.2 ka and 24.0 ± 2.0 ka from [Lei et al. \(2022\)](#). These suggest two events ruptured the entire Bayanhaote fault. In fact, the three paleoearthquakes were revealed from the dip-slip deformation in the reverse zone in this study, and there are insufficient records to effectively identify paleoearthquakes related to the strike-slip zone in the trench. We infer that the three paleoearthquakes revealed in this study were only a part of these events. Although [Jing et al. \(2019\)](#) published more paleoearthquakes in the southern section, the current paleoearthquake data are insufficient to establish a complete recurrence model for the entire fault.

Seismotectonic model around the Helan Mountains

The tectonic deformation around the Helan Mountains was the product of the interaction between the Alxa and Ordos blocks. Based on GPS and stress field observations, the two blocks were under oblique compression with dextral shear along the north–south-trending boundary. The boundary zone consists of the active Bayanhaote Basin, Yinchuan Basin, and Helan Mountains. The Helan Mountains are triangular, and the hypotenuse of this triangle in the southeast is the Yinchuan Basin, which is controlled by a succession of normal faults running from NE to SW. The Bayanhaote Basin and Jilantai Basin lie to the west and north, respectively. The boundary zone between the Alxa and Ordos blocks was simplified into a structural model, as shown in [Figure 5](#).

A study on the sedimentation of the Yinchuan Basin showed that the NE–SW trending Yinchuan Basin is controlled by a normal fault system under depression and receiving sediments ([Wang et al., 2007](#); [Guo et al., 2017](#)). Cenozoic sediments are thick in the northwest part ([Cai and Zhou, 2018](#); [Yang and Dong, 2018](#); [Yang and Yang, 2018](#)). With the deep seismic reflection profiles across the Helan Mountains and Yinchuan Basin, the lithospheric structure of this region was revealed, and a negative flower structure was proposed as the geometric combination of normal faults ([Fang et al., 2009](#); [Liu et al., 2017](#)). The published data show that the total vertical slip rate of the SE-dipping east Helanshan and Luhatai faults in the Yinchuan Basin is greater than that of the NW-dipping Yinchuan–Pingluo fault and Yellow River faults ([Lei, 2016](#)), and the Helan Mountains are relatively uplifted ([Liu et al., 2010](#)). We believe that the SE-dipping normal fault system on the west side of the Yinchuan Basin should not be cut and limited by the Yellow River fault in-depth and should extend downward to cut the interfaces between the upper and lower crust and the Moho interface. This model provides a better explanation for the depression at the Moho interface ([Fang et al., 2009](#); [Chen et al., 2020](#)). The tectonic status of the Bayanhaote Basin changed from the Mesozoic to Cenozoic. The main active tectonics were transferred from the basin-bounding normal faults to the inner-basin strike–slip fault ([Yang and Dong, 2018](#)). The Bayanhaote fault developed as a new boundary fault. As a strike–slip fault, the fault could not extend eastward and connect to the Yinchuan Basin fault system. We believe that it directly cuts down the entire lithosphere and becomes a new block boundary between Alxa and Ordos. This updated tectonic model ([Figure 5](#)) integrating current data on the deep structure and fault kinematics provides a new interpretation of the shallow-to-deep structure in the boundary zone between the Alxa and Ordos blocks.

In this regional tectonic model centered around the Helan Mountains, the Luoshan fault is a relatively simple boundary structure between the Alxa and Ordos blocks in the Luoshan area. The right-lateral slip rate of the Luoshan fault (~4.3 mm/a) is considered to represent the relative movement between the Alxa and Ordos blocks ([Middleton, et al., 2016b](#)). The GPS stations west of the Bayanhaote fault advance northward at a rate of 2.0–2.5 mm/a relative to the Ordos block ([Hao et al., 2021](#)), which approximates the relative movement of the two blocks. These GPS values are similar to the geological data from the Luoshan fault. [Lei \(2016\)](#) calculated a 1.05-mm/a N–S strike–slip caused by the extension of the NE-trending normal faults in the Yinchuan Basin. We may derive a dextral strike–slip rate of about 1.0–1.5 mm/a on the Bayanhaote fault by deducting the slip of the Yinchuan Basin from the overall motion between the Alxa and Ordos blocks, which is close to the dextral strike–slip rate of 1.0–2.4 mm/a obtained from a field investigation in this study. Based on the slip rate, length of the Bayanhaote fault, and normal fault system in the Yinchuan Basin, we infer that the Bayanhaote fault may have the seismogenic capability and seismic risk similar to that of normal fault systems in the Yinchuan Basin.

Conclusion

Data from offset landforms and trench profiles at the site south of Sumutu show that the northern section of the Bayanhaote fault was dominated by right-lateral strike–slip. It also had some reverse slip, which resulted in the relative uplift of the western plate and the formation of a semi-flower structure in the shallow sediments. Based on the ~137 m dextral strike–slip of landforms and the OSL dating data from the trench, we estimated the dextral strike–slip rate of the fault to be 1.0–2.4 mm/a. This estimation of the slip rate was compared with that published by prior studies in the southern section and was consistent with the relative movement between the Alxa and Ordos blocks.

The analysis of strata and faulting in the trench found that three strong earthquakes with significant reverse slips were recorded in the reverse zone within the 18-m-wide fault zone. These events occurred between 56.28 ± 4.04 ka and 55.33 ± 3.04 ka, between 32.79 ± 2.22 ka and 13.76 ± 1.1 ka, and between 13.76 ± 1.1 ka and 7.86 ± 0.43 ka, with a reverse slip of 0.44, 0.35, and 0.29 m, respectively. The deformation distribution in the trench suggested that there were more than three paleoearthquakes. More study is needed to develop a comprehensive paleoearthquake recurrence model for the entire Bayanhaote fault.

We developed a regional tectonic model around the Helan Mountains, including the Bayanhaote fault developed in the Bayanhaote Basin west of the Helan Mountains, by integrating the sedimentation and activity of the normal fault system in the

Yinchuan Basin east of the Helan Mountains. This implies that the Bayanhaote fault was capable of producing strong earthquakes with similar magnitude as the normal fault system in the Yinchuan Basin. The Bayanhaote fault, along with the normal fault system in the Yinchuan Basin on the east side of the Helan Mountains, constitutes the boundary structural belt between the Alxa and Ordos blocks and absorbs the majority of the dextral shear deformation of the two blocks along the N–S boundary.

Data availability statement

The original contributions presented in the study are included in the article/Supplementary Material; further inquiries can be directed to the corresponding author.

Author contributions

GC: conceptualization, funding acquisition, investigation, formal analysis, and writing. ZL: investigation and formal analysis. XH: formal analysis, review, and editing.

Funding

This study was supported by the National Key Research and Development Program of China (Grant No. 2018YFC1504201).

References

- Bi, H., Zheng, W., Lei, Q., Zeng, J., Zhang, P., and Chen, G. (2020). Surface slip distribution along the west helanshan fault, northern China, and its implications for fault behavior. *J. Geophys. Res. Solid Earth* 125 (7), e2020JB019983. doi:10.1029/2020JB019983
- Cai, L., and Zhou, J. (2018). Development characteristics of the fault system in Yinchuan Basin and its control action on the Basin. *Pet. Geophys.* 16 (2), 53–59.
- Chen, G., Zeng, X., Li, Z., and Xu, X. (2022). Active faulting of landforms along the tuosihu-maoniushan fault and its seismotectonic implications in eastern qaidam basin, China. *Seismol. Res. Lett.* 93, 897–913. doi:10.1785/0220210110
- Chen, Y., Chen, J., Guo, B., Li, S., Qi, S., Zhao, P., et al. (2020). Crustal structure and deformation between different blocks in the northern part of the western margin of Ordos. *Chin. J. Geophys.* 63 (3), 886–896. doi:10.6038/cjg2020N0211
- Cowgill, E. (2007). Impact of riser reconstructions on estimation of secular variation in rates of strike-slip faulting: Revisiting the Charchen River site along the Altyn Tagh Fault, NW China. *Earth Planet. Sci. Lett.* 254 (3), 239–255. doi:10.1016/j.epsl.2006.09.015
- Deng, Q., Cheng, S., Min, W., Yang, G., and Reng, D. (1999). Discussion on Cenozoic tectonics and dynamics of Ordos block. *J. Geomechanics* 5 (3), 13
- Fang, S.-M., Zhao, C.-B., Chai, C.-Z., Liu, B.-J., Feng, S.-Y., Liu, M.-J., et al. (2009). Seismic evidence of crustal structures in the Yinchuan faulted basin. *Chin. J. Geophys.* 52 (7), 1768–1775. doi:10.3969/j.issn.0001-5733.2009.07.010
- Guo, X. Y., Jiang, C. S., Wang, X. S., and Tian, X. (2017). Characteristics of small to moderate focal mechanism solutions stress field of the Circum-Ordos block. *J. Geodesy Geodyn.* 37 (7), 675–685.
- Hao, M., Wang, Q., Zhang, P., Li, Z., Li, Y., and Zhuang, W. (2021). “Frame Wobbling” causing crustal deformation around the Ordos Block. *Geophys. Res. Lett.* 48, e2020GL091008. doi:10.1029/2020GL091008

Acknowledgments

OSL samples were dated in the OSL Laboratory of the National Institute of Natural Hazards, Emergency Management Department. We would like to thank Zhao Junxiang for her help with sample testing. We thank Erdente Gus from the Civil Affairs Bureau of Alxa Zuoqi and Chen Hongbo from Yinchuan for coordinating land use for trench excavation. We are grateful to Shiming Zhang and Feng Li for their helpful discussions and suggestions. We also appreciate helpful comments from the reviewers and the editor Daoyang Yuan.

Conflict of interest

The authors declare that the research was conducted in the absence of any commercial or financial relationships that could be construed as a potential conflict of interest.

Publisher's note

All claims expressed in this article are solely those of the authors and do not necessarily represent those of their affiliated organizations, or those of the publisher, the editors, and the reviewers. Any product that may be evaluated in this article, or claim that may be made by its manufacturer, is not guaranteed or endorsed by the publisher.

- Huang, X. N., Zhang, J. S., Li, T. B., Liu, F., and Feng, J. (2012). Characteristics of active faults between the north segment of the north–south seismic belt and the central Mongolia. *Seismol. Geol.* 34 (4), 637–658. doi:10.3969/j.issn.0253-4967.2012.04.009

- Jing, Z. J., Xie, F. R., Zhang, S. M., Du, Y., Huang, X. M., and Zhang, L. (2019). Database and report of active fault mapping of the Bayanhaote Fault. Available at: https://www.activefault-datacenter.cn/data_share (Accessed 05 Oct 2021).

- Lei, Q. Y. (2016). *The extension of the arc tectonic belt in the northeastern margin of the Tibet plateau and the evolution of the Yinchuan Basin in the western margin of the North China*. (Beijing: Institute of Geology, China Earthquake Administrator). Doctoral Thesis.

- Lei, Q., Yu, J., Zhang, P., Zheng, W., Zhang, Z., Du, P., et al. (2022). Tectonic geomorphology and prehistoric earthquakes of the West Helanshan fault, West Ordos, and its implications for regional tectonics and seismic hazard. *Tectonophysics* 833, 229375. doi:10.1016/j.tecto.2022.229375

- Liu, B., Feng, S., Ji, J., Wang, S., Zhang, J., Yuan, H., et al. (2017). Lithospheric structure and faulting characteristics of the Helan mountains and yinchuan Basin: Results of deep seismic reflection profiling. *Sci. China Earth Sci.* 60 (3), 589–601. doi:10.1007/s11430-016-5069-4

- Liu, J., Zhang, P., Zheng, D., Wan, J., Wang, W., Du, P., et al. (2010). Pattern and timing of late Cenozoic rapid exhumation and uplift of the helan mountain, china. *Sci. China Earth Sci.* 53 (3), 345–355. doi:10.1007/s11430-010-0016-0

- Liu, S., and Liu, X. (2002). Structural types and its relation with oil and gas of bayanhot basin. *J. Southwest Petroleum Univ. Sci. Technol. Ed.* 24 (3), 24–27. doi:10.3863/j.issn.1000-2634.2002.03.007

- Ma, J., and He, D. (2019). Meso-Cenozoic tectonic events in the Helanshan Tectonic Belt and its adjacent areas: constraints from unconformity and fission

track data. *Acta Petrol. Sin.* 35 (4), 1121–1142. doi:10.18654/1000-0569/2019.04.10

Middleton, T. A., Walker, R. T., Parsons, B., Lei, Q., Zhou, Y., and Ren, Z. (2016a). A major, intraplate, normal-faulting earthquake: The 1739 yinchuan event in northern China. *J. Geophys. Res. Solid Earth* 121 (1), 293–320. doi:10.1002/2015JB012355

Middleton, T. A., Walker, R. T., Rood, D. H., Rhodes, E. J., Parsons, B., Lei, Q., et al. (2016b). The tectonics of the western ordos plateau, ningxia, China: slip rates on the luoshan and east Helanshan faults. *Tectonics* 35 (11), 2754–2777. doi:10.1002/2016TC004230

Murray, A. S., and Wintle, A. G. (2000). Luminescence dating of quartz using an improved single-aliquot regenerative-dose protocol. *Radiat. Meas.* 32, 57–73. doi:10.1016/S1350-4487(99)00253-X

Research Group on Active Fault System around Ordos Massif (1988). *Active fault system around ordos massif*. Beijing, China: Seismological Press.

Sheng, S.-Z., Wan, Y.-G., Huang, J.-C., Bu, Y.-F., and Li, X. (2015). Present tectonic stress field in the circum-Ordos region deduced from composite focal mechanism method. *Chin. J. Geophys.* 58 (2), 436–452. doi:10.6038/cjg20150208

Tapponnier, P., Xu, Z. Q., Roger, F., Meyer, B., Arnaud, N., Wittlinger, G., et al. (2001). Oblique stepwise rise and growth of the Tibet Plateau. *science* 294 (5547), 1671–1677. doi:10.1126/science.105978

Wang, X.-S., Lü, J., Xie, Z.-J., Long, F., Zhao, X.-Y., and Zheng, Y. (2015). Focal mechanisms and tectonic stress field in the North-South seismic belt of china. *Chin. J. Geophys.* 58 (11), 4149–4162. doi:10.6038/cjg20151122

Wang, Y., Du, P., and Lei, Q. Y. (2007). Summary on recent progress of active fault exploration project in Yinchuan City. *Technol. Earthq. Disaster Prev.* 2 (2), 166–175.

Wei, Z., He, H., Lei, Q., Sun, W., and Liang, Z. (2021). Constraining coseismic earthquake slip using structure from motion from fault scarp mapping (East Helanshan Fault, China). *Geomorphology* 375, 107552. doi:10.1016/j.geomorph.2020.107552

Xu, X., Han, Z., Yang, X., Zhang, S., Yu, G., Zhou, B., et al. (2016). *Seismotectonic map in China and its adjacent regions in Chinese*. Beijing: Seismological Press. doi:10.12031/activefault.china.250.2016.dbXU

Yang, X., and Dong, Y. (2018). Mesozoic and cenozoic multiple deformations in the helanshan tectonic belt, northern China. *Gondwana Res.* 60, 34–53. doi:10.1016/j.gr.2018.03.020

Yang, Y., and Yang, W. (2018). Quaternary distribution characteristics of Yinchuan basin based on electrical characteristics. *Ningxia Eng. Technol.* 17 (1), 15–19.

Yuan, D.-Y., Ge, W.-P., Chen, Z.-W., Li, C.-Y., Wang, Z.-C., Zhang, H.-P., et al. (2013). The growth of northeastern tibet and its relevance to large-scale continental geodynamics: A review of recent studies. *Tectonics* 32 (5), 1358–1370. doi:10.1002/tect.20081

Zhang, J., Cunningham, D., Yun, L., Qu, J., Zhao, H., Zhang, B., et al. (2021). Kinematic variability of late cenozoic fault systems and contrasting mountain building processes in the Alxa block, western China. *J. Asian Earth Sci.* 205, 104597. doi:10.1016/j.jseas.2020.104597